Optimization of Antenna Structure Design

R. Levy
Ground Antenna and Facilities Engineering Section

Optimality criteria design is applied for large antenna structures with multiple constraints on microwave performance. The constraints are on accuracy of the structure: restrictions on the microwave pathlength error, and the antenna pointing error. The examples given show convergence to low-weight feasible designs that satisfy the constraints. Truss-member sizes are automatically selected from tables of commercially available structural shapes, and approximations resulting from the method of selection are found moderate. The multiple constraint design is shown to be more effective in meeting constraints than the old envelope method. For practical structures, the new design method can be performed within reasonable core size and computation time.

I. Introduction

Structure design optimization theory and its application to a number of classical or academic problems have been described in the past two decades (14). Consequently, there are now theoretical design approaches to obtain low-weight structure designs that satisfy a variety of constraints on structure performance and safety. In particular, design approaches that use optimality criteria (Refs. 1, 6, 7, 10, and 15) are feasible for the design of structures with large numbers of degrees of freedom and/or design variables.

This article describes a specific application of the optimality criteria method to design structures that satisfies constraints on compliance, member tension, and buckling stresses. The model contains several thousand members and degrees of freedom and tens to hundreds of design variables, substantially more than encountered in design optimization models described in research literature. The emphasis here is on the design of a microwave antenna backup structure for which the design variables are the areas of the truss rod members or the thicknesses of membrane plates. Microwave performance constraints limit: (a) the root-mean-square of microwave pathlength deviations from a surface that is a best fitting alternative to the originally specified surface and (b) the antenna boresight pointing error. These constraints are functions of the displacements of the nodes of the structure that support reflective surface panels and must be satisfied for gravity and wind-pressure loadings at specified operational wind speeds. Stress and buckling constraints for gravity and operational wind-speed loadings tend to be benign, but can become significant at higher wind-speed survival conditions, or at other nonoperational environmental conditions.

The following discussions provide a brief review of the optimality criteria method and the pathlength error constraint. A new method that formulates pointing error constraints is introduced. A practical selection of structural members from tables of commercially available shapes is also described. Results from trial designs are given for the new 34-m (112-ft) diameter ground DSN antenna shown in Fig. 1. Histories of the design progress and comparisons of the efficiencies between the simple sequential envelope method designs and new designs that treat multiple constraints simultaneously are given. Another example compares the selection of design variables from commercial shape tables with the traditional assumption of a continuous spectrum of shapes.

II. Problem Formulation

Large ground antennas are essentially membrane-type structures in which the finite elements are rods (major) and plates (minor). Consequently, only the three translational degrees of freedom for displacements and forces at the structure nodes are needed. For brevity, only rod element areas (design variables) with identical material properties are discussed. The extensions to include the thicknesses of membrane plates as additional types of design variables and to treat members of different materials are straightforward (Refs. 7, 11, and 13).

A. Optimality Criteria Method

A brief formulation is provided for background. Further details, variations, and implementation strategies are available in the literature (Ref. 1, 7, 10, 13, and 15).

The key components of an optimization problem formulation are the objective function and the constraints. Here, the design objective is to minimize structure weight, or equivalently, volume, given as

$$V = \sum_{i=1}^{N} L_i a_i \tag{1}$$

in which a_i is the cross-sectional area, L_i is the length, and i is the index within a set of N design variables. Primary constraint equations are expressed as

$$G_j = \sum_{i=1}^{N} \frac{F_{ij} L_i}{a_i} - C_j^* \leqslant 0 \qquad j = 1, \cdots, K \tag{2}$$

In Eq. (2), F_{ij} is a sensitivity coefficient such that the virtual work of the ith design variable for the jth constraint is $F_{ij}L_i/a_i$. When the design variable group consists of only a single member, the sensitivity coefficient is the product of the stress resultant (bar force) for a specified external loading and the stress resultant for an associated virtual (dummy) loading divided by Young's modulus. When the group contains more than one member, the length-weighted average product is used to compute the coefficient, and the length assigned to the group is the total length of members. C_j^* is a prespecified bound on the virtual work. In particular, when the displacement in a particular direction at a given node is the constraint, then C_j^* is that displacement bound and the virtual load is a unit load applied at that node and in that direction. Stress constraints for rod members can be converted to extension constraints, and the virtual loading vector consists of a pair of collinear self-equilibrating loads applied at the terminal nodes of the member. Antenna pathlength or pointing error constraint virtual loadings consist of particular vectors with components at all nodes that support surface panels.

Secondary constraints on the design variables can be imposed as

$$\underline{a}_i \leqslant a_i \leqslant \bar{a}_i \qquad i = 1, \cdots, N \tag{3}$$

in which $\underline{a}_i$ and $\bar{a}_i$ are either user-established lower and upper bounds on the design variable a_i or dynamic adjustments constructed by algorithm. A possible replacement for a primary stress constraint is a lower bound side constraint developed by the stress ratio method. The replacement could produce significant computational savings and is valid for members that are not strongly affected by structural redundancy.

Equation (2) can be written as

$$G_j = C_j - C_j^* \tag{4}$$

where C_j is the realized value of the virtual work for the jth constraint and is given by the summation term of Eq. (2).

It is useful to define a constraint ratio, D_j, for which values greater than unity indicate an unsatisfied constraint. This can be computed as

$$D_j = C_j / C_j^* \tag{5}$$

The optimality criteria for the design variables for this problem are

$$a_i^2 = \sum_{j=1}^{K} F_{ij} \lambda_j \qquad j = 1, \cdots, K \tag{6}$$

in which the λ_j are nonnegative Lagrangian multipliers to be determined from solution of the following auxiliary problem:

$$\lambda_j G_j = 0 \qquad j = 1, \cdots, K \tag{7}$$

Strategies for solution of Eq. (7), typically either by Newton's method or a recursive approximation, have been discussed elsewhere (Refs. 5, 6, 10, and 15).

The sensitivity coefficients, F_{ij}, are assumed to be independent of the design variables, but structural redundancy weakens this assumption, so that the design must be approached iteratively through a number of cycles in which the sensitivity coefficients are recomputed. In the case of antenna gravity loading, the loads are a function of the design variables, which reinforces the need for iterative design. "Move" limits are often imposed upon the relative changes in design variables between adjacent cycles in an attempt to control the effects of redundancy or loading changes. These are invoked by adjustments to the upper and lower bounds on design variables as expressed in Eq. (3).

B. Antenna Pathlength Constraints

Microwave pathlength errors are determined from the original geometry of the surface and the deflection vectors of the surface nodes. Figure 2 shows the surface geometry relationships. The solid line through the antenna vertex represents the original ideal paraboloidal surface, and the broken line represents the deflected surface. The microwave pathlength is defined as the distance from the aperture plane to the surface plus the distance from the surface (after reflection) to the focal point and is shown by line *BCP*. In the figure, *GD* is the deflection vector and *dn* is the component of the deflection vector normal to the surface. It can be shown (Ref. 17) that the half-pathlength error R is given by

$$R = (BCP - ADP)/2 = \gamma_z \, dn \tag{8}$$

where γ_z is the direction cosine of the surface normal with respect to the focal (Z) axis.

In practice, the pathlength errors are computed from an alternative paraboloid that best fits the deflected surface. The best-fitting paraboloid is defined by at most six parameters, i.e., there are three independent shifts of the vertex parallel to the Cartesian X, Y, or Z coordinate axes, one relative change in focal length, and two independent rotations, one about the X (parallel to elevation) axis and the other about the Y (yaw) axis. Then the vector of pathlength errors $\mathbf{R}$ with respect to the best-fitting surface can be computed as follows:

$$\mathbf{R} = \mathbf{A}\,\mathbf{u} + \mathbf{B}\,\mathbf{h} \tag{9}$$

in which $\mathbf{u}$ is an external loading displacement vector for the nodes that support surface panels and the components of $\mathbf{u}$ are aligned parallel with the Cartesian axes, $\mathbf{h}$ is the vector of fitting parameters, and $\mathbf{A}$ and $\mathbf{B}$ are invariant matrices that contain the geometric relations to transform $\mathbf{u}$ and $\mathbf{h}$ as required by Eq. (8). Equation (9) is used as the basis of a least squares analysis (Ref. 17) to derive $\mathbf{h}$. In particular, we find

$$\mathbf{h} = \mathbf{H}\,\mathbf{u} \tag{10}$$

in which $\mathbf{H}$ is again an invariant matrix derived from $\mathbf{A}$ and $\mathbf{B}$ and is equal to

$$\mathbf{H} = -(\mathbf{B}^t \mathbf{W} \mathbf{B})^{-1} \mathbf{B}^t \mathbf{W} \mathbf{A} \tag{11}$$

where $\mathbf{W}$ is a diagonal matrix of weighting factors usually taken to be proportional to the aperture area tributary to each surface node.

It has been shown (Ref. 8) for a pathlength error constraint that the virtual loading vector consists of loads directed normal to the antenna surface at each node that supports surface panels. The magnitudes of the loads are $\gamma_z^2 \, dn$, where *dn* is with respect to the best-fit paraboloid. When this loading is employed, the realized virtual work will become the sum of squares of half-pathlength errors and will be identical to the error computed by the usual geometric analysis of the deflections.

It is common to refer to the "rms error" of a paraboloidal antenna by the root-mean-square half-pathlength error from the best-fitting paraboloid. This is derived from the weighted sums of squares and the sums of the weighting factors.

In the cases of gravity loading, the pathlength errors at particular antenna elevation angles are computed for the difference in loading between that elevation and the "rigging" angle elevation. The "rigging" angle is the angle at which the panels are aligned in the field as accurately as possible to the ideal surface. Also, a single gravity loading can be constructed to define an appropriate constraint to represent either the maximum or a weighted average rms antenna pathlength error over the range of elevations from horizon to zenith. For either of these choices, there is an implicit computer algorithm (Ref. 9) to determine the rigging angle. Figure 3 illustrates different pathlength error distribution curves from horizon to zenith for different choices of rigging angle.

C. Antenna Pointing Constraints

Five independent additive components that contribute to the antenna boresight pointing error can be derived from geo-

metric optics theory (Ref. 12) for Cassegrain antennas. Definitions of the associated terms and the computational relationships are contained within Table 1. The first two rows of multiplying factors in the table apply to parameters of the best-fit paraboloid that can be extracted from the vector **h** that was defined in conjunction with Eqs. (9) and (10). However, as seen from Eq. (10), the inner product of each row of **H** with the displacement vector for external loading provides the corresponding term of **h**. Therefore, the virtual loading is derived from the appropriate rows of **H** multiplied by the factors of the table. As **H** is invariant, it needs to be computed only once for each structure, and it applies to all pointing constraints.

The virtual loads for the remaining pointing error contributions, which are in the last three rows of the table, are constructed from loads placed at the nodes that define the rotation and translations of subreflector and feed. The magnitudes of these loads are the tabulated factors times the coefficients of the equation used to define the rotation or translation. For example, if the feed translation is defined as the average displacement of two particular nodes in, say, the Y coordinate direction, the virtual loading consists of loads in the Y direction at these two nodes with magnitudes of 0.5 times the factor $k/(mf)$. Furthermore, if part of the pointing error is correctable by feedback from a sensor or encoder, subtractive virtual loading components can be included so that virtual work derived from this vector will provide the net pointing error. The virtual loading vector for each constraint is the union of the components constructed for each contribution to the pointing error.

III. Candidate Design Variables

The selection of structural members is usually restricted to a discrete set of commercially available cross-sectional shapes. Nevertheless, the optimality criteria (Eq. 6) assume a continuous spectrum for selection of design variables; consequently, a rigorous approach would employ a different design method (Refs. 2 and 16) to deal with the discrete spectrum. The approach used here, however, is to perform the design first for a continuous spectrum and then choose the nearest available size that also meets lower bound stress side constraints. This approach could theoretically lead to a nonoptimal selection, but if the available shapes provide a well-graduated set of properties without significant gaps, the departures from the optimal selection should become insignificant.

Figure 4 is a sample from one of several tables constructed for design within the JPL-IDEAS computer program. This particular table contains pipe and round-tube customary shapes. Since these tables are assembled from local warehouse stock lists, the data is in customary U.S. units. Under the heading HANDBOOK SHAPE, there is an abbreviated description of the section. For example, entry number 2 is a 1-in. (25.4-mm) schedule 10 pipe with 1.315-in (43.9-mm) outside diameter and 0.109-in. (2.7-mm) wall thickness. The cross-sectional area and radius of gyration are tabulated under the headings AREA and RAD. The load table contains allowable compression loads in kips (4,448 N) for the span lengths listed at the top. These loads are based upon the buckling stress formulas for ASTM A-36 steel in the ASCE design guide (Ref. 4). The design tension stress is also based upon the design guide, but the allowable loading can be reduced by a percentage to correct for reduced cross sections at connected ends.

The table is used to set the lower bound side constraint for compressive loads by using member length, maximum load for all loading cases, and the buckling stress formula. The nearest shorter-span-length column is searched for the first section with a larger allowable load, and the buckling formula is applied to determine the allowable load using the member length with the area and radius of gyration of the identified section. If the section is found to be inadequate, the section in the next lower row of the table is tested until an adequate shape is found. The shapes are listed in the table in the order of increasing area so that the search finds the lightest member to carry the load. Allowable loads tabulated as zero indicate that the slenderness ratio for that entry would be greater than an arbitrary limit of 200. The table is also used in each cycle after execution of the design algorithm to find the shape consistent with the lower bound side constraint that is closest in area to the one determined by optimality criteria.

IV. Example Applications

Structure models for the 34-m antenna examples that follow are extracted from design studies of NASA DSN antennae (Fig. 1) scheduled to be installed in California and Australia in 1985. Design optimization will be described only for the tipping structure, which consists of quadripod, reflector backup structure, and elevation wheel. Design of the alidade, which supports the tipping structure at the elevation bearings and at the elevation-wheel pinion, is relatively simpler and is not described here.

The tipping structure analytical model contains approximately 1145 nodes, 3400 unconstrained displacement degrees of freedom, 3900 rod members, and 90 membrane plates, and is redundant to about the 500th degree. The quadripod contains about 200 nodes and consists of four towerlike legs connected to an apex structure that supports the subreflector. The backup structure (Fig. 5) consists of 24 main and 24 secondary radial rib trusses, 12 circumferential hoop trusses, and other bracing. Parasitic reflective surface panels that support only their own weights and local surface loads are attached to

450 front nodes of the rib trusses. Eight of the main rib trusses are connected to and are supported by an octagonal frame of the elevation-wheel structure.

The elevation wheel (Fig. 6) contains about 50 nodes, provides the transition from backup structure to alidade, and supports the elevation-wheel bull gear. Backup structure and elevation-wheel structures are redundantly connected at eight points, which complicates their design. Design of the quadripod members is less affected by redundant coupling. Individual bar and plate member elements are grouped for fabricational convenience into 190 distinct design variable groups.

A. Design for Performance Constraints

Simultaneous rms pathlength and pointing error constraints are imposed for gravity and wind loadings. The antenna rigging angle is established to make the pathlength errors for gravity loading equal at horizon and zenith antenna elevations.

The design example here is subjected to the nine pathlength and pointing error constraints listed in Table 2. These nine constraints are known to be the most demanding for this model. No primary stress constraints are imposed; all stress requirements are treated as side constraints with minimum sizes established, as described previously, from commercial shape tables.

Although the performance constraints are specified for operational wind speeds of 13.4 m/s (30 mph), the structure must withstand wind speeds of 31.2 m/s (70 mph) at any orientation and 44.7 m/s (100 mph) when stowed at the zenith elevation. To satisfy these requirements, the wind-pressure loadings applied for design are at the higher wind speeds, and the allowable value for the constraint is increased accordingly.

The computer run was limited to six analysis cycles and five design cycles. Figure 7(a) shows the cyclic progression histories of structure weight and of the most severe constraint ratio. Note that the designs at cycles 1, 2, and 4 are not feasible because of constraint ratios greater than unity. Nevertheless, the discrepancy at cycle 4 between actual and predicted constraint ratios indicates that the design procedure operated correctly in cycle 3 by developing a design with a predicted constraint ratio of unity. Unfortunately, the effect of structural redundancy produces the unanticipated response in cycle 4. The move limit used to control redundancy is equal to 1.5, which requires each design variable to be at least 2/3 and not more than 3/2 of its value in the prior cycle. A smaller move limit could have overcome part of the excessive constraint ratio at cycle 4, but would have caused additional problems at cycle 2. The predicted constraint ratio here is greater than unity because the move limit activated a sufficient number of side constraints to prevent the free choices of the design variables necessary to satisfy the optimality criteria.

Figures 7(b) and (c) show the cyclic constraint ratio histories for the four pathlength error constraints and for the five pointing error constraints. These figures show the dichotomy of pointing and pathlength error performance. One example of this is seen at cycle 4, where the gravity pathlength error constraint is exceeded although the pointing error constraint is satisfied. Another example is the 0° elevation, 120° yaw wind-loading case; the pointing error constraint is always active, and yet, except for the first cycle, the pathlength error constraint never is. Nevertheless, the design in Fig. 7 is successful because there was no increase in structure weight from the first to the sixth design cycle, and all nine excessive constraint ratios at the first cycle became feasible at the sixth.

A more erratic design history is shown in Fig. 8. The structure model is analogous to but slightly larger than the previous and has two more constraints. The effect of redundancy is emphasized by the relatively large move limit of 2.0. This is assumed to be responsible for the significant constraint violations at cycles 2, 3, 5, and 6 since the predicted constraint ratios, which were close to unity at cycles 3 through 6, indicate successful execution of the design procedure. In particular, the design at cycle 4, which is 15% lighter than the initial, is feasible because the large initial constraint ratio has been reduced to unity.

B. Discrete Versus Continuous Design Variables

A design that chooses the nearest available discrete shape to approximate the assumed continuous spectrum for design variables is compared with a design based upon a continuous spectrum. The 16-cycle histories shown in Fig. 9 are for design of the backup structure of a hypothetical 40-m antenna. Sizes of the design variables for the continuous design case are determined by the optimality criteria whenever the lower bound side constraint does not control; but whenever stress or maximum slenderness ratio governs the selection, the appropriate discrete size is chosen. The small move limit of 1.25 was used in an attempt to obtain smooth convergence. The normalized structural weights plotted were obtained after feasibility scaling, which consisted of multiplying the structure weight by the largest constraint ratio for constraint ratios greater than unity. The figure shows that the small differences in weight in the early cycles tend to disappear as the designs approach convergence.

C. Multiple Constraint Versus Envelope Method Designs

The last example compares designs obtained by solving for the Lagrangian multipliers simultaneously to satisfy the mul-

tiple constraint conditions of Eq. (7) with the old envelope method (Refs. 1 and 3). The envelope method uses sequential explicit decoupled solutions for the Lagrangian multipliers and applies the optimality criteria to each solution. The final selection of design variables at each design cycle is the envelope of maximum values obtained from the decoupled solutions.

The example is for a 34-m antenna tipping structure model similar to the one described at the beginning of this section, but with only seven primary pathlength and pointing error constraints. The design history in Fig. 10(a) shows similar structural weights achieved for the fourth through sixth cycles. Figure 10(b) shows that both methods have overcome significant first-cycle violations of the first, fourth, and fifth constraints and that the two methods appear to be equivalent for the third through seventh constraint ratios. But at the sixth cycle, the envelope method is not feasible because of the first and second constraints, while the multiple constraint method is feasible for all seven constraints. Computer run times were about the same for both methods.

V. Computer Resources

Problem size and storage capacity for the JPL-IDEAS computer program is primarily limited by the requirement of keeping a triangular matrix of maximum wavefront size in core during stiffness matrix decomposition. The 34-m antenna problem has a maximum wavefront of 220 degrees of freedom, which requires core storage for about 55,000 36-bit words to contain the double-precision decomposition triangle and associated pointers. Program source code and other storage bring the total requirement to 110,000 words. The design program operates on a UNIVAC 1100/81 computer, which can provide at least twice this in-core storage. Therefore, problems about 50% larger than this could be processed by the present program.

One complete design cycle uses 348 central processing unit (cpu) seconds. Of these, 90 s are associated with the design problem: 83 s are used for constructing and solving the pathlength and pointing error virtual loading vectors, and the remaining 7 s are used to determine the Lagrangian multipliers and apply the optimality criteria. Furthermore, the 83 s for vector processing appears to be excessive and could be reduced significantly by improvement of the present program.

One cycle for statics analysis with no provisions for design would require 336 s. This time is derived by subtracting the 90 s used for design and adding 78 s used during a preamble phase of the program to read and provide initial processing of input data. The following times, in cpu seconds, are used for analysis: stiffness matrix decomposition, 209; load-displacement vector processing, 40; stress resultant recovery, 5; pathlength and pointing error analysis, 4. A total of 2157 cpu seconds is used for the six cycles of Fig. 7.

VI. Summary

The optimality criteria method is reviewed for design of large ground antennas with performance constraints on microwave pathlength errors. The formulation is extended to include constraints on antenna boresight pointing errors simultaneously with the pathlength constraints.

Examples drawn from practice show that significant performance improvements and low structure weight are achieved within as few as six cycles of computer analysis and redesign. Furthermore, optimization was found not to extend maximum core size requirements and adds only a moderate increase in the cpu time for a design cycle beyond that of a "standard" analysis cycle. This implies that computer-automated design optimization run times could be less than 10 times that for a single analysis cycle.

A practical method is described to automate selection of structural member design variables from a discrete table of commercially available structural shapes. An example comparison of a discrete shape design with a design that assumed a continuous spectrum shows no major discrepancies for the approximations of discrete selection.

An example comparison of the older envelope design method with the present simultaneous multiple constraint design method shows that, although the designed structure weights are almost the same, the envelope method violates two of the seven performance constraints.

References

1. Berke, L., and N. Khot, "Use of Optimality Criteria Methods for Large Scale Systems," AGARD Lecture Series No. 70, *On Structural Optimization*, Hampton, Va., Oct. 1974, pp. 1–29.

2. Cella, A., and R. Logcher, "Automated Optimum Design from Discrete Components," *Journal of the Structural Division*, Proc. ASCE 97 (ST–1), Proc. Paper 7845, Jan. 1971, pp. 175–189.

3. Gellatly, R., L. Berke, and W. Gibson, "The Use of Optimality Criteria in Automated Structural Design," 3rd Conference on Matrix Methods in Structural Mechanics, WPAFB, Ohio, Oct. 1971.

4. *Guide for Design of Steel Transmission Towers*, ASCE Manual and Report on Engineering Practice, No. 52, 1971.

5. Kamat, M., and R. Hayduk, "Recent Developments in Quasi-Newton Methods for Structural Analysis and Synthesis," AIAA/ASME/ASCE/ACS 22nd SDM Conference, Paper 0576, Atlanta, Ga., Apr. 6–8, 1981.

6. Khot, N., L. Berke, and V. Venkayya, "Comparison of Optimality Structures by the Optimality Criterion and Projection Method," AIAA/ASME/SAE 20th SDM Conference, Paper 79–0720, St. Louis, Mo., Apr. 4–6, 1979.

7. Khot, N., L. Berke, and V. Venkayya, "Comparison of Optimality Criteria Algorithms for Minimum Weight Design of Structures," *AIAA Journal*, Vol. 17, No. 2, Feb. 1979, pp. 182–190.

8. Levy, R., and R. J. Melosh, "Computer Design of Antenna Reflectors," *Journal of the Structural Division*, Proc. ASCE 99 (ST-11), Proc. Paper 10178, Nov. 1973, pp. 2269–2285.

9. Levy, R., "Antenna Bias Rigging for Performance Objective," IEEE Mechanical Engineering in Radar Symposium, Wash. D.C., Nov. 8–10, 1977.

10. Levy, R., and W. Parzynski, "Optimality Criteria Solution Strategies in Multiple Constraint Design Optimization," *AIAA Journal*, Vol. 20, No. 5, May 1982, pp. 708–715.

11. Levy, R., "Computer-Aided Design of Antenna Structures and Components," *Computers and Structures*, Vol. 6, 1976, pp. 419–428.

12. Rusch, W., and P. Potter, *Analysis of Reflector Antennas*, Academic Press, New York, London, 1970.

13. Sander, G., and C. Fleury, "A Mixed Method in Structural Optimization," *International Journal for Numerical Methods in Engineering*, Vol. 13, 1978, pp. 385–404.

14. Schmit, L., "Structural Synthesis: Its Genesis and Development," *AIAA Journal*, Vol. 19, No. 10, Oct. 1981, pp. 1249–1263.

15. Schmit, L. A., and C. Fleury, "Structural Synthesis by Combining Approximation Concepts and Dual Methods," *AIAA Journal*, Vol. 18, No. 10, Oct. 1980, pp. 1252–1260.

16. Schmit, L. A., and C. Fleury, "Discrete-Continuous Variable Structural Synthesis Using Dual Methods," *AIAA Journal*, Vol. 18, No. 12, Dec. 1980, pp. 1515–1524.

17. Utku, S., and S. M. Barondess, *Computation of Weighted Root-Mean-Square of Path Length Changes Caused by the Deformation and Imperfections of Rotational Paraboloidal Antennas*, Technical Memorandum 33–118. Jet Propulsion Laboratory, Pasadena, Calif., Mar. 1963.

List of Symbols

a	cross-sectional area
$\underline{a}$	lower limit on area
$\overline{a}$	upper limit on area
C^*	prespecified maximum value of constraint
C	computed value for constraint in current design
D	constraint ratio
dn	normal component of distortion vector
F	sensitivity coefficient
G	constraint equation
L	length
R	half-pathlength error
V	volume
γ	direction cosine of the surface
λ	Lagrangian multiplier

Vectors and Matrices

$\underline{\mathbf{u}}$	displacement vector
$\mathbf{h}$	vector of fitting parameters
$\mathbf{A}$	geometric transformation matrix
$\mathbf{B}$	geometric transformation matrix
$\mathbf{H}$	invarient matrix as defined in Eq. (11)
$\mathbf{W}$	weighting matrix (diagonal)

Subscripts

i	design variable index
j	constraint index
z	reference to the Z axis

Table 1. Cassegrain antenna pointing error contributions

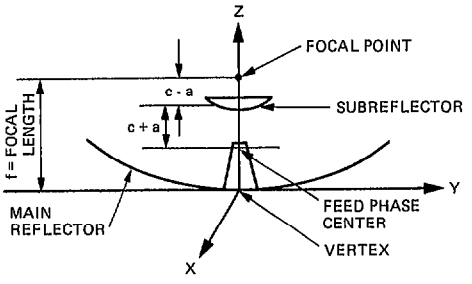

Definitions

k = beam deviation factor ($k \sim 0.75$)

m = magnification factor

$m = (c+a)/(c-a)$

($m \sim 5.0 - 10.0$)

Contributing displacement	Factor	
	X axis	Y axis
Best-fit paraboloid		
Vertex shift	$-k/f$	k/f
Rotation	$1+k$	$1+k$
Subreflector		
Lateral translation	$(1-1/m)k/f$	$-(1-1/m)k/f$
Rotation	$-2(c-a)k/f$	$-2(c-a)k/f$
Feed		
Lateral translation	$k/(mf)$	$-k/(mf)$

Pointing Error = Σ (Displacement × Factor)

Table 2. Performance constraints

Condition			Half-pathlength root-mean-square, mm (in.)	Pointing, arc seconds
Wind, m/s (mph)	Elevation, degrees	Yaw, degrees		
13.4 (30)	0	120	0.330 (0.0130)	30.0
13.4 (30)	60	180	0.330 (0.0130)	30.0
13.4 (30)	90	90	0.330 (0.0130)	30.0
13.4 (30)	90	180	None	30.0
Gravity-worst case: horizon to zenith			0.165 (0.0065)	75.0

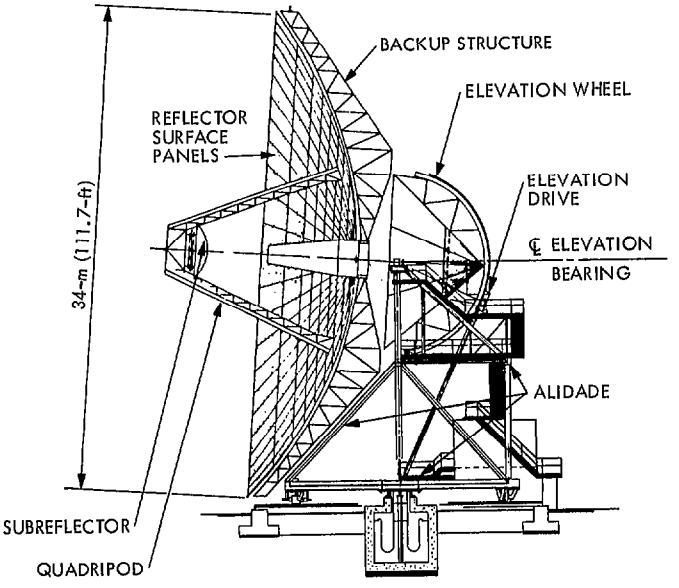

Fig. 1. 34-meter Deep Space Network antenna

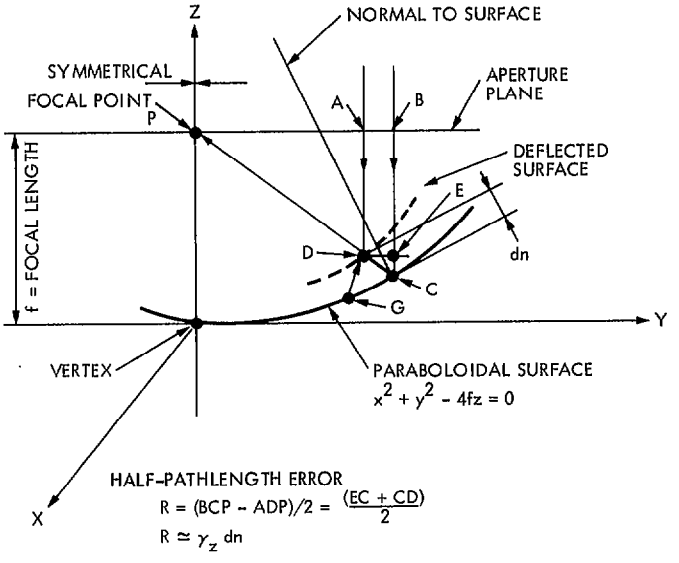

Fig. 2. Surface deflection geometry

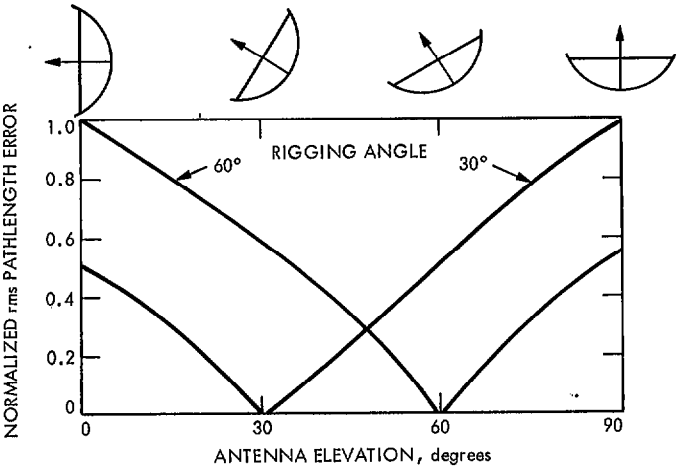

Fig. 3. Pathlength error distribution vs rigging angle

HANDBOOK PROPERTIES FOR PIPES

HANDBOOK NO. SHAPE	AREA	RAD	******LOAD TABLE****** SPAN LENGTHS 25.	50.	75.	100.	125.	150.	175.	200.
1).75STD, 1.05X.113	.333	.330	8.4	4.1	.0	.0	.0	.0	.0	.0
2)1.0-10, 1.315X.109	.413	.430	11.2	8.3	3.9	.0	.0	.0	.0	.0
3)1.0STD, 1.315X.133	.494	.420	13.3	9.8	4.4	.0	.0	.0	.0	.0
4)1.25-10, 1.66X.109	.531	.550	15.0	12.4	8.2	4.6	.0	.0	.0	.0
5)1.5-10,1.90X.109	.613	.630	17.7	15.2	12.2	7.0	4.5	.0	.0	.0
6)1.25STD, 1.66X.140	.669	.540	18.8	15.5	9.9	5.6	.0	.0	.0	.0
7)2.0-10, 2.375X.109	.776	.800	22.9	20.6	17.9	14.2	9.1	6.3	.0	.0

Fig. 4. Excerpt from common member shape table

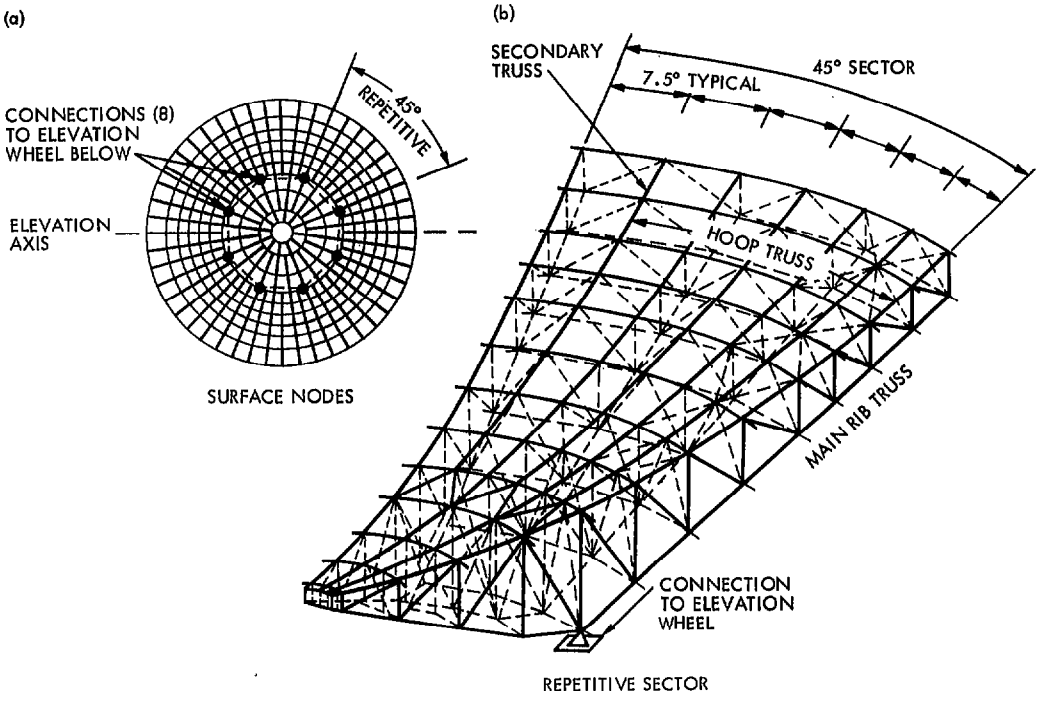

Fig. 5. 34-meter antenna backup structure: (a) surface nodes; (b) repetitive sector

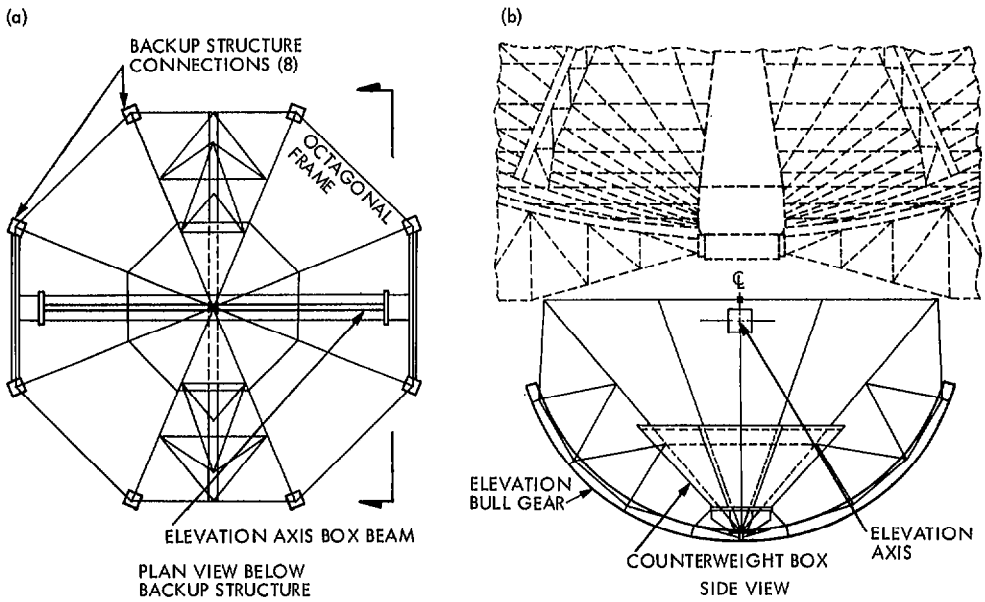

Fig. 6. 34-meter antenna elevation wheel: (a) plan view below backup structure; (b) side view

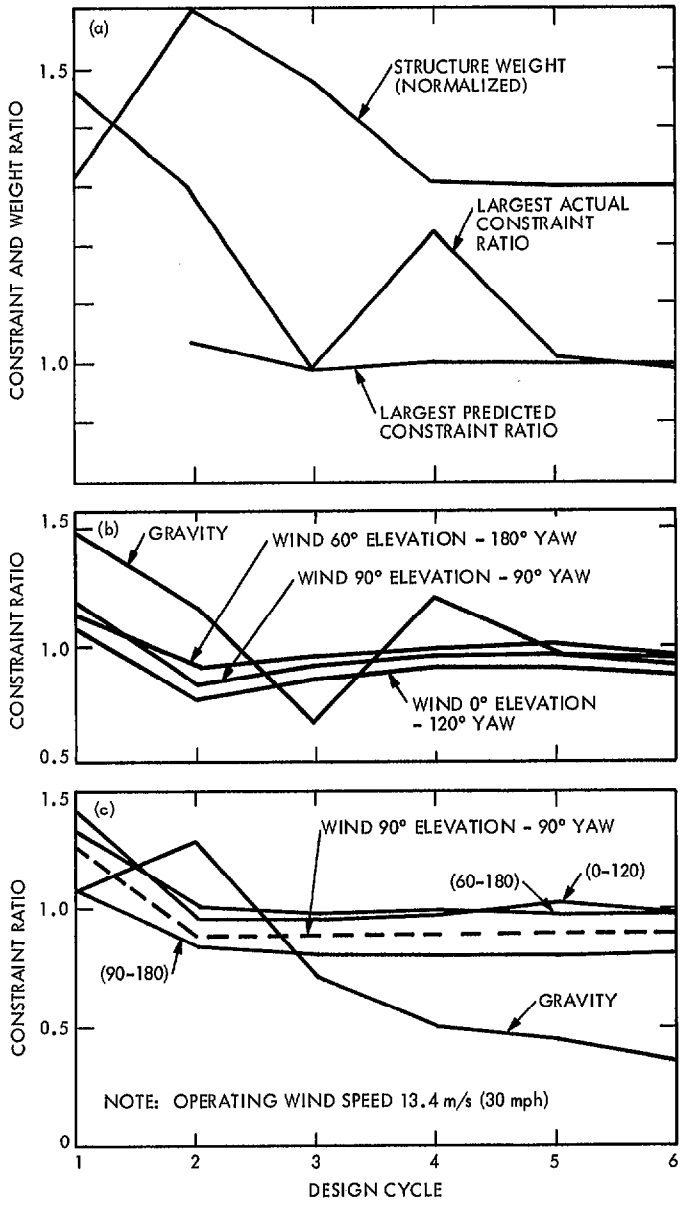

Fig. 7. 34-meter antenna tipping structure design history: (a) weight and controlling constraint ratios; (b) pathlength error constraint ratios; (c) pointing error constraint ratios

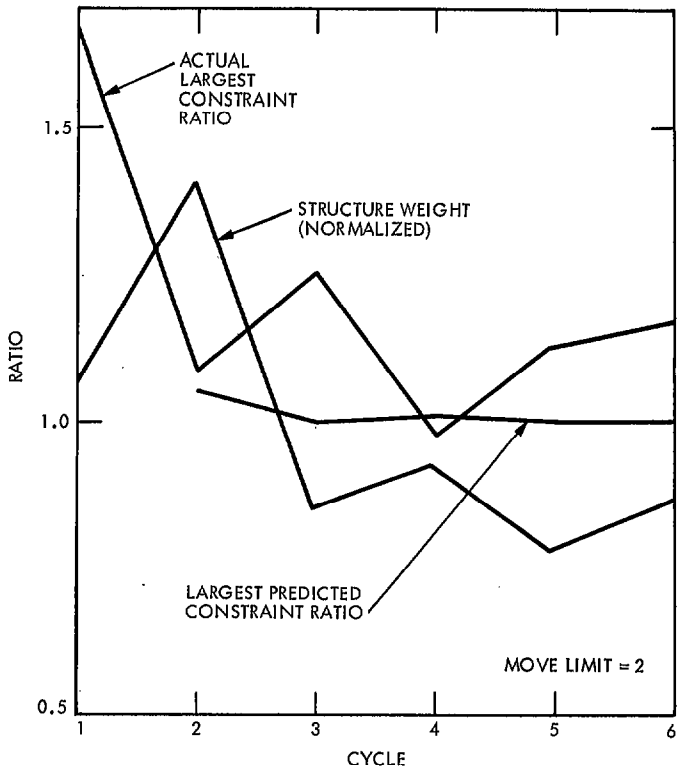

Fig. 8. 34-meter antenna cyclic weight and constraint ratio history, move limit = 2.0

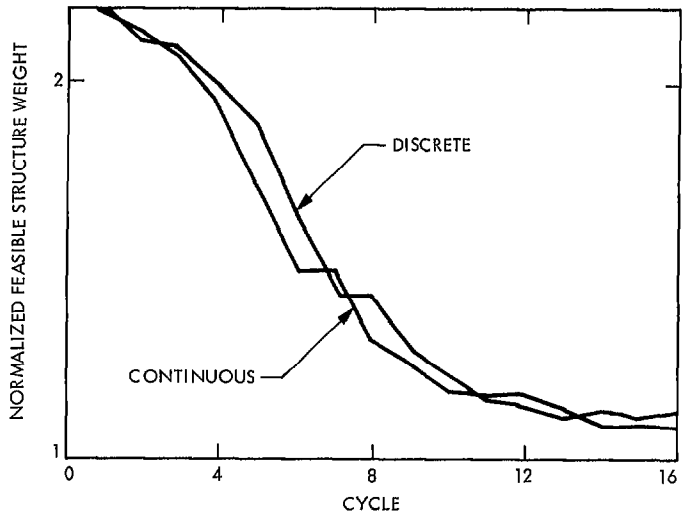

Fig. 9. 40-meter backup structure designs: discrete vs continuous design variables

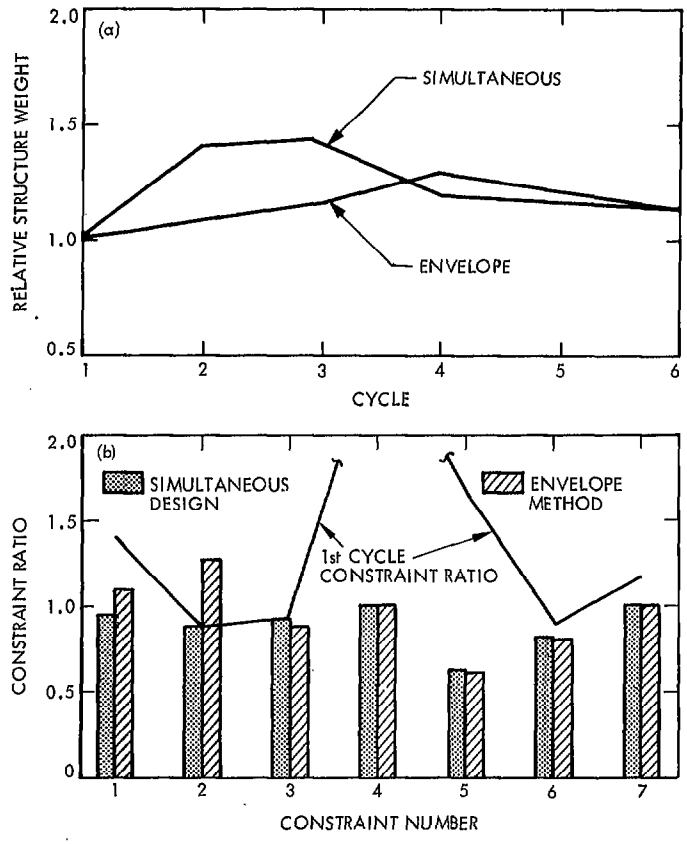

Fig. 10. 34-meter antenna simultaneous multiple constraint envelope method designs: (a) structure weight history; (b) sixth cycle primary constraint ratios